

Article

Centimeter-Level Precise Orbit Determination for the LuoJia-1A Satellite Using BeiDou Observations

Lei Wang ^{1,2}, Beizhen Xu ^{1,*}, Wenju Fu ¹, Ruizhi Chen ^{1,2}, Tao Li ¹, Yi Han ¹ and Haitao Zhou ¹

¹ State Key Laboratory of Information Engineering in Surveying, Mapping and Remote Sensing, Wuhan University, Wuhan 430079, China; lei.wang@whu.edu.cn (L.W.); wenjufu@whu.edu.cn (W.F.); ruizhi.chen@whu.edu.cn (R.C.); tao.li@whu.edu.cn (T.L.); yi_han@whu.edu.cn (Y.H.); haitao.zhou@whu.edu.cn (H.Z.)

² Collaborative Innovation Center for Geospatial Technology, Wuhan 430079, China

* Correspondence: beizhen_xu@whu.edu.cn; Tel.: +86-15527155902

Received: 1 June 2020; Accepted: 21 June 2020; Published: 26 June 2020



Abstract: LuoJia-1A is a scientific experimental satellite operated by Wuhan University, which is the first low earth orbiter (LEO) navigation signal augmentation experimental satellite. The precise orbit is the prerequisite of augmenting existing Global Navigation Satellite System (GNSS) performance and improves users' positioning accuracy. Meanwhile, LEO precise orbit determination (POD) with BeiDou-2 observations is particularly challenging since it only provides regional service. In this study, we investigated the method of precise orbit determination (POD) for LuoJia-1A satellite with the onboard BeiDou observation to establish the high-precision spatial datum for the LEO navigation augmentation (LEO-NA) system. The multipath characteristic of the BeiDou System (BDS) observations from LuoJia-1A satellite is analyzed, and the elevation-dependent BeiDou code bias is estimated with the LEO onboard observations. A weight reduction strategy is adopted to mitigate the negative effect of poor BeiDou-2 geostationary earth orbit (GEO) satellites orbit quality, and the LuoJia-1A orbit precision can be improved from 6.3 cm to 2.3 cm with the GEO weighting strategy. The precision improvement of the radial direction, along-track, and out-of-plane directions are 53.47%, 47.29%, and 76.2%, respectively. Besides, tuning the pseudo-stochastic parameters is also beneficial for improving orbit precision. The experiment results indicate that about 2 cm overlapping orbit accuracy are achievable with BeiDou observations from LuoJia-1A satellite if proper data processing strategies are applied.

Keywords: LuoJia-1A satellite; BeiDou observations; precise orbit determination; reduce-dynamic; navigation augmentation

1. Introduction

Low-Earth-Orbiter (LEO) satellites have been used widely for space applications such as gravity field measurement, high-resolution images, synthetic-aperture laser radar, and Global Navigation Satellite System (GNSS) radio occultation [1–3]. Apart from these traditional scientific missions, LEO satellites have also risen in the communication as well as navigation mission in recent years [4]. Recently, the LEO navigation augmentation (LEO-NA) technology has been considered as a promising technique to reduce the slow convergence issue in GNSS precise positioning [5,6].

The LEO satellite navigation augmentation technology includes the signal-based augmentation and information based augmentation [7]. The LEO satellite navigation signal augmentation method is achieved by generating and broadcasting the ranging signals to users, whereas the information augmentation method is achieved by transmitting the GNSS corrections information using the LEO

satellite communication channels. Some research has demonstrated that the LEO satellite signal augmentation method can dramatically reduce the convergence time of Precise Point Positioning (PPP) [8] as well as long-baseline real-time kinematic (RTK) positioning by taking the advantages of the rapid geometric change of LEO satellites [9,10]. Moreover, it also can improve the usability and reliability of the present Global Navigation Satellite System (GNSS) and supporting the Positioning Navigation Timing (PNT) systems as well as the space-based real-time Positioning, Navigation, Timing, Remote-sensing, and Communication (PNTRC) information service systems [11,12].

Luojia-1A satellite is operated by Wuhan University, which was launched in June 2018 to carry out the LEO-based navigation signal augmentation experiment. The experiment was successful, and its initial performance has been assessed from a different perspective [5,13]. As for the LEO navigation signal augmentation system, it is critical to maintaining the precise orbit and time systems as well as operating the precise and stable ranging signals to users. Therefore, LEO precise orbit determination (POD) is of great importance to the LEO navigation signal augmentation system. Presently, the reduced-dynamic POD method using GPS observations has been extensively studied and widely used in many LEO satellites. Since demonstrated centimeter-level orbit precision of the TOPEX/POSEIDON satellite with onboard GPS observations [14], various LEO missions have achieved high precision with the GPS-based POD, such as CHAMP, GRACE, GOCE, and SWARM [15–18].

The BeiDou system consists of geostationary earth orbit (GEO) satellites, inclined geostationary (IGSO) satellites, and medium earth orbit (MEO) satellites, which is going to provide the global navigation services in 2020 [19,20]. With the emerging BeiDou system, there is only a few LEO satellites carried BeiDou receiver for orbit determination. The LINGQIAO satellite, a mobile communication experimental satellite in China, equipped with a Beidou system (BDS) receiver, demonstrated the initial performance of BDS based orbit determination [21]. The major challenge for BeiDou-based LEO POD is the poor precision of the GEO satellite precise orbit. The Chinese meteorological satellite FengYun-3C achieved centimeters-level POD with the BeiDou system by excluding the GEOs observations [22]. Zhang, et al. [23] improved the BDS based precise orbit result of FengYun-3C with the calibration of orbit biases in BeiDou GEO satellites. However, the strategies of BDS-based LEO POD are still far from fully understood.

In this study, we make use of BDS dual-frequency observations from the Luojia-1A satellite to investigate the BDS based LEO POD methods. Firstly, the Luojia-1A satellite is briefly introduced, including the satellite-body-fixed (SBF) system. Secondly, the visibility and continuity of onboard BDS measurements are analyzed. The BDS elevation-dependent code biases are modeled with the Luojia-1A observations. Then, the optimal weighting strategy for BeiDou-based LEO POD as well as the optimal precise orbit determination strategy is investigated.

2. Luojia-1A Satellite Platform

Luojia-1A is a small scientific experimental satellite with night light remote sensing and LEO signal navigation augmentation functions. The weight of the satellite is 19.8 kg, and its size is $520 \times 870 \times 390$ mm. Luojia-1A satellite is operated in a sun-synchronous orbit at 645 km. The outlook of Luojia-1A satellite is illustrated in Figure 1, three GNSS antennas were installed: two of them are used to receive GPS/BDS dual-frequency signals in the opposite direction, and one antenna is used to transmit the navigation augmentation signals to users. Besides, a night light camera and a satellite communication antenna are installed on the +Z side of the satellite. Luojia-1A satellite can receive the GPS/BDS dual-frequency signals and provide autonomous orbit and timing information onboard and transmit dual-frequency ranging signals to the users.

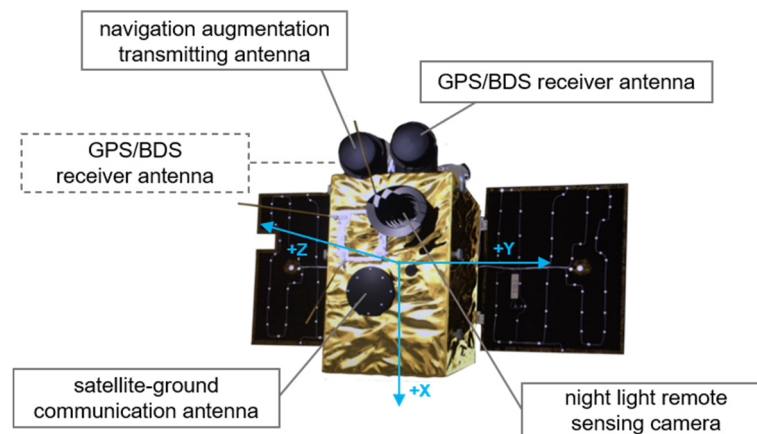


Figure 1. The appearance of the Luojia-1A satellite.

A satellite-body-fixed (SBF) coordinate system of Luojia-1A is established for LEO POD, which is the right-handed coordinate system. The origin of the SBF system is at the center of mass (COM) of the satellite. The +X axis is aligned to the satellite velocity direction. The +Z axis points to the optical camera, and the +Y axis is perpendicular to the XOZ plane. Moreover, two receive antennas of Luojia-1A are in the +Z and $-Z$ direction, respectively. The +Z axis point to the earth during the data transferring, and the solar panel is kept facing the sun in standby mode. The small size of the satellite body makes the offset between the GNSS antennas and the satellite COM at the decimeter level, which is smaller than most satellites. The satellite attitude mode of the Luojia-1A satellite is also special since the satellite keeps its solar panel facing the sun to receive more solar power, and it turns its +Z side facing to the earth during the mission period. Most navigation satellites always keep their +Z side toward the earth since they continuously transmit navigation signals. Hence, the Luojia-1A satellite is more complicated, which also affects the BeiDou signal tracking.

3. BeiDou Multipath Modeling with Luojia-1A Observations

The high-quality BeiDou observations are the prerequisites of LEO POD. Hence, we analyzed the BeiDou observations from the Luojia-1A satellite before starting the orbit determination procedure.

3.1. Data Collection

In this study, the Luojia-1A onboard BDS data of 2018 DOY 159 were collected with a 1-s sample rate. The onboard BDS data include both B1I and B2I frequency data. To demonstrate the effectiveness of BDS based orbit determination, the onboard BDS observations of Luojia-1A are analyzed in this section.

The statistical details of BDS observations are shown in Figure 2. The left panel shows the number of observations tracked during the observation period, and the right panel shows the percentage of three types of BeiDou satellites. The observation condition of the Luojia-1A satellite depends on the altitude of the satellite. The figure indicates that the Luojia-1A tracks the most observations from the C03 and the C07 satellites. Regarding the observation ratio, it concludes that the observations from the GEO satellite contribute to 42.18%, which is nearly the same as IGSO satellites. It should be noticed that GEO and IGSO satellites contribute to more than 80% observations, while these satellites are only available in Asia–Pacific and surrounding regions. The MEO satellites contribute fewer observations due to fewer MEO satellites and faster change of relative geometry between MEO and LEO satellites.

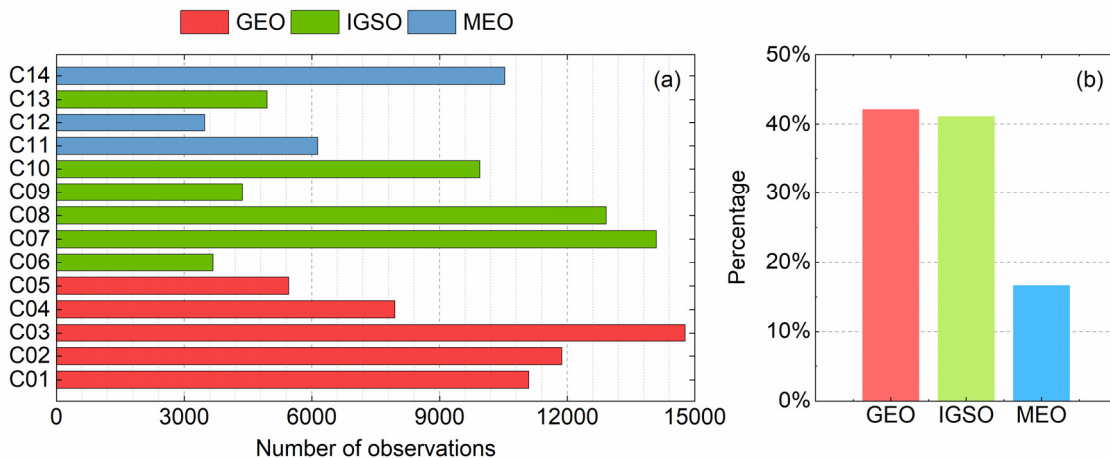


Figure 2. Statistics of BDS observations. (a) The number of observations for BDS satellites. (b) The percentage of different BeiDou satellite types.

The onboard BDS receiver equipped on the Luojia-1A satellite supports 12 channels for each frequency, which is abundant for Beidou-2 signal tracking. As the BeiDou-3 satellite deployment, more channels are necessary for future receivers capable of tracking BeiDou-2 and BeiDou-3 signals. The time series of observed satellite number of the epoch and its statistic results are shown in Figure 3. The figure indicates that the Luojia-1A suffers mild intermittent interruption during BDS satellite signals tracking, and the reason is worth further investigation. The right panel indicates that the Luojia-1A can track five or seven satellites per epoch in most cases. There is only a 57.8% chance for Luojia-1A to track more than four BDS satellites simultaneously. This is mainly because most BeiDou satellites are located above the Asia-Pacific region, which is also challenging for obtaining continuous and precise orbit with only Beidou-2 observations.

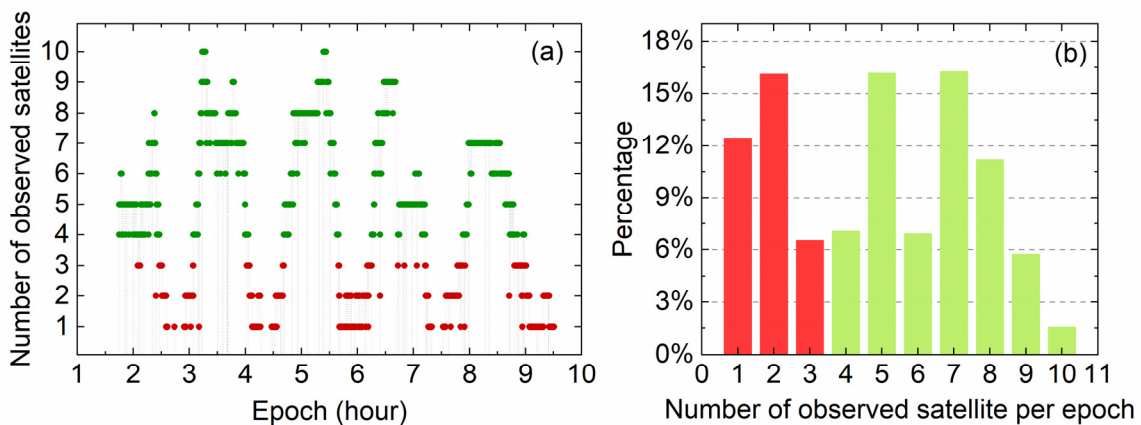


Figure 3. The number of observed satellites (a) and the statistic result (b).

The sky view of GEO satellites, IGSO satellites, and MEO satellites from the Luojia-1A is shown in Figure 4. In the figure, different colors mean different satellite types. The sky view of the BDS satellites is relative to the antenna reference frame (ARF) of the Luojia-1A satellite. The azimuth angle is started from the +X axis in the SBF. Referring to the sky view of C02 and C03 satellites, it is apparent that the Luojia-1A has a better observational condition for GEO satellites without a noticeable data breach. As for the C08 satellite, the azimuth varies from 0° to 180°, and the observations are more concentrated. Moreover, there are data outages of the C10 satellite observation arc. As for the MEO satellites shown in the figure, the observation arc is shorter than that of GEO and IGSO satellites, and the continuity is not as good as that of GEO and IGSO satellites.

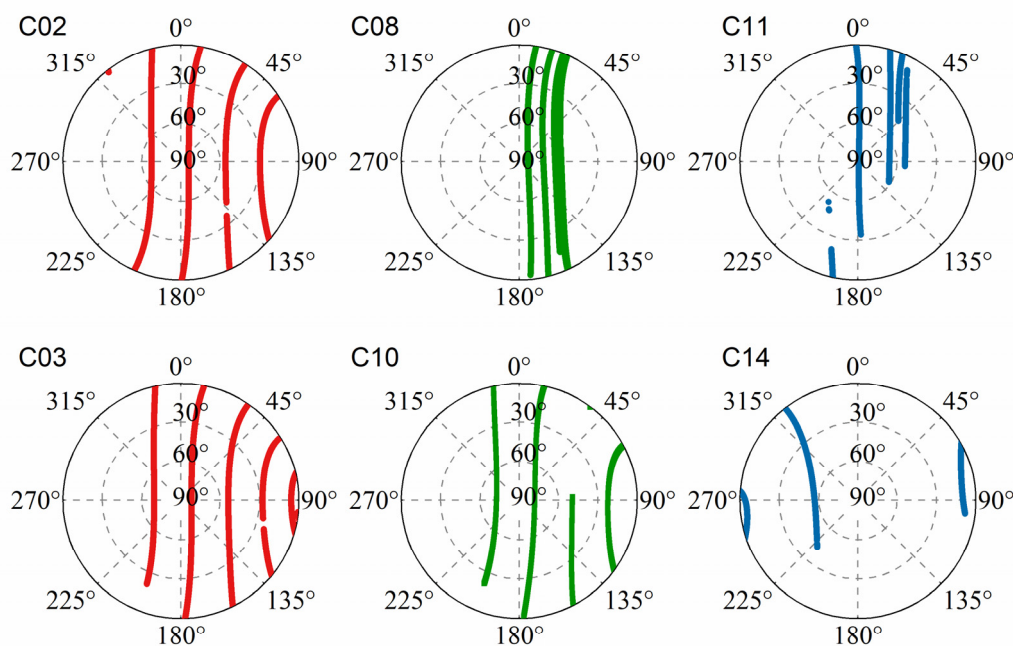


Figure 4. The sky view of the BeiDou satellites from the ARF of Luojia-1A satellite. The red, green, and blue lines represent the geostationary earth orbit (GEO), inclined geostationary (IGSO), and medium earth orbit (MEO) satellites, respectively.

3.2. Modeling the Multipath of BeiDou Observations

The pseudorange observations of BeiDou are reported as suffering from the elevation-dependent multipath biases, which may lead to an adversary impact on positioning accuracy [24]. Currently, the elevation-dependent code variations of BDS-2 IGSO and MEO satellites are based on the data from ground stations. The ground stations are not able to capture the elevation-dependent biases for the GEO satellites, due to a stable geometry relationship. The LEO onboard BDS observations can be used to capture the geometric change of the GEO satellites, which can be used as a complementary approach for the multipath biases modeling. The multipath error can be estimated with the linear combination of code and carrier-phase observations, which can be expressed as follows [25,26]:

$$MP_i = C_i - \frac{f_i^2 + f_j^2}{f_i^2 - f_j^2} \lambda_i \varphi_i + \frac{2f_j^2}{f_i^2 - f_j^2} \lambda_j \varphi_j + \frac{f_i^2 + f_j^2}{f_i^2 - f_j^2} \lambda_i N_i - \frac{2f_j^2}{f_i^2 - f_j^2} \lambda_j N_j - D_c \quad (1)$$

where C and φ represent the code and carrier-phase observables, respectively. The f is the frequency, λ is the wavelength, and N represents the carrier phase ambiguity. The subscripts i, j ($i \neq j$) are used to specify different frequencies; D_c is the constant part of hardware delays.

The BDS code bias was analyzed based on Luojia-1A onboard measurements. In this section, the MP1 and MP2 represent the code multipath of B1 and B2 frequency. The MP1 and the elevation of several BDS satellites are shown in Figure 5, which indicates that most BeiDou satellites present systematic elevation-dependent variations in multipath combination. According to the GEO satellites, such as the C02 and C05, it is obvious that the multipath is decreased as the elevation increases. As for the IGSO satellite, e.g., C07, the trend is similar to the GEO satellites but with a more dramatic variation. Another IGSO satellite, the C10 satellite, has a low elevation, so it has a larger multipath bias without an obvious trend. Considering the MEO satellites, the multipath is linearly increasing as the elevation angle decreases, which is shown in panel (c). The multipath error of the C14 satellite is generally smaller than 2 m without significant elevation-dependent variation.

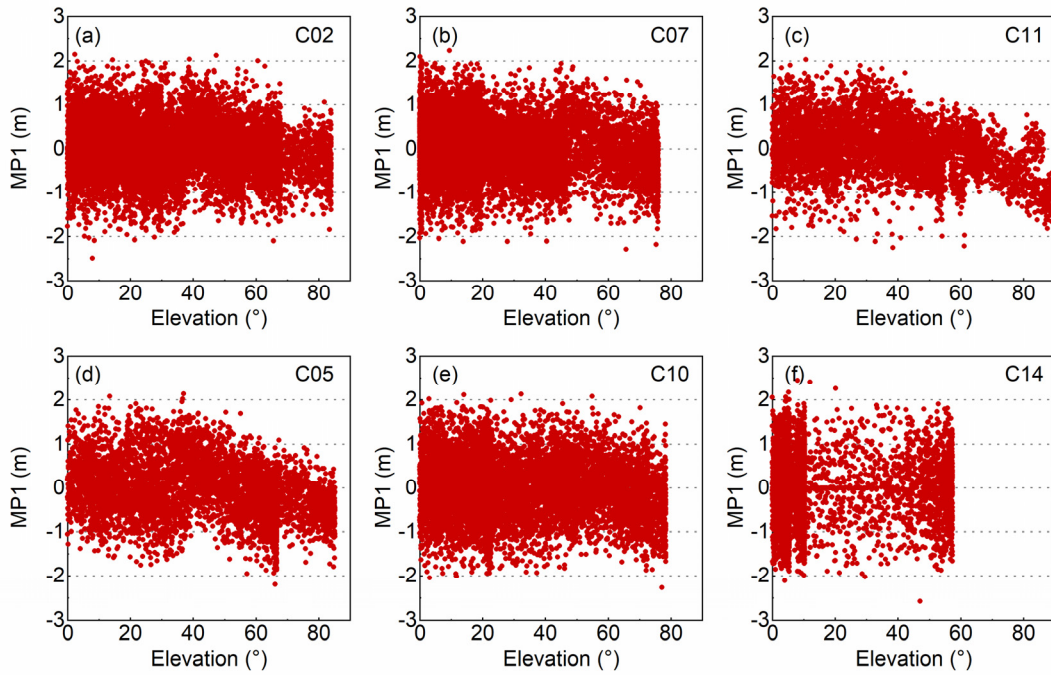


Figure 5. The relationship between multipath and antenna elevation angle for different BDS satellites: (a) C02, (b) C07, (c) C11, (d) C05, (e) C10, (f) C14.

To mitigate the impact of multipath biases, an elevation-dependent model is established with the BeiDou observations from the Luojia-1A satellite. The elevation-dependent modeling method proposed by Wanninger and Beer [24] is adopted in this study for the multipath (MP) series. To define the piecewise linear models for MP series, the elevations interval, which varies from 0° to 90° , is split by 10 nodes with the spacing of 10° . Therefore, the values of 10 nodes are estimated for the elevation-dependent model, and the restriction that the average of model values is zero. The MP observables with the elevation e between e_k and e_{k+1} can be expressed as follows:

$$MP_f^s(e) = \left(\frac{e - e_k}{e_{k+1} - e_k} \right) P_{f,k+1}^s + \left(1 - \frac{e - e_k}{e_{k+1} - e_k} \right) P_{f,k}^s + v_i \quad (2)$$

where f represents the frequency and s is the type of the BeiDou satellites. There is a 10° difference between e_k and e_{k+1} . $P_{f,k}^s$ and $P_{f,k+1}^s$ are the MP values of the contiguous grid point, which are estimated using the methods of least square estimation.

Figure 6 shows the elevation-dependent MP models, which are built respectively for the GEO, IGSO, and MEO satellites for both B1 and B2 frequencies. The results from Wanninger and Beer [24] are also presented in the figure for comparison. The upper panels of the figure represent the model for the B1 signal. It is obvious that the MP1 models of the Luojia-1A satellite are elevation-dependent, which is marginal below the 40° and gradually decreased as the elevation increase after 40° . According to the panels (b) and (c), the MP1 models of the Luojia-1A satellite are similar to that of the Wanninger model above 40° , especially the model of the MEO satellites. However, since the results of the Luojia-1A satellite also include the satellite-induced MP effects, there are still minor differences. On the other hand, as shown in the lower panels, there is no elevation dependence for the MP2 models of the Luojia-1A satellite, which shows a slow decrease after 60° . The obvious differences between MP1 and MP2 models may be attributed to the Luojia-1A receiver that can smooth the BeiDou B2 signal. The MP models built from the Luojia-1A onboard observations are not as smooth as the Wanninger model, which may be because the Wanninger model adopts much longer observed time. The MP models can be used to correct the pseudorange measurements directly for the single-frequency orbit determination of LEO satellites.

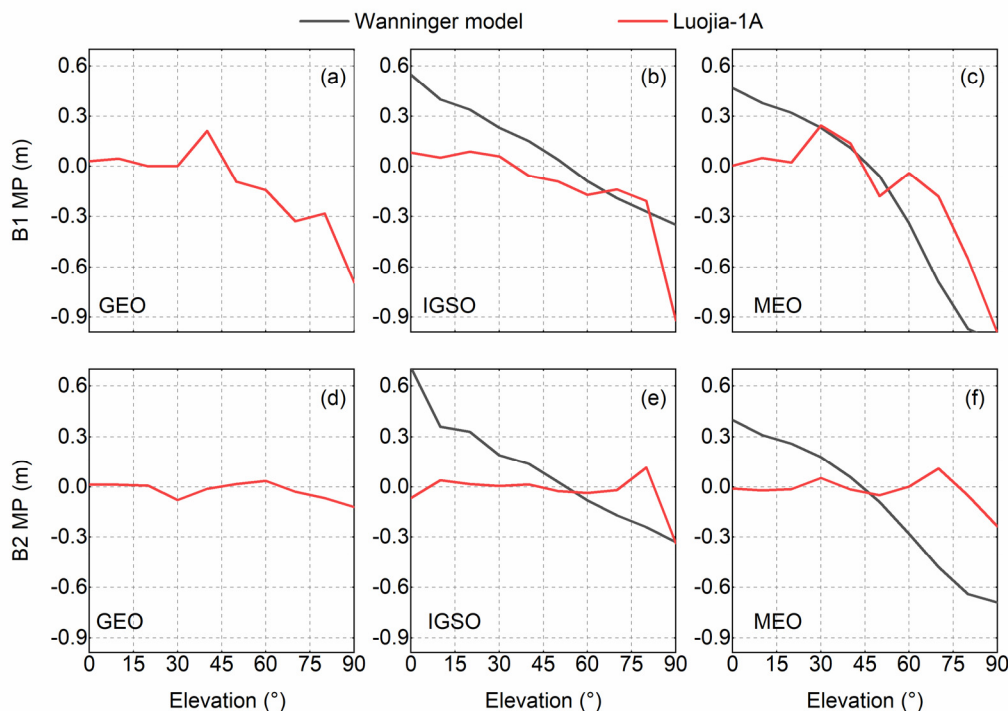


Figure 6. The elevation-dependent multipath models for the GEO, IGSO, and MEO satellites. The upper and the bottom panels represent models for B1 and B2 respectively.

4. Methodologies for the Beidou-Based LEO POD

There are a few challenges in BeiDou-based LEO POD, including the BeiDou GEO orbit error handling and tuning the pseudo-stochastic parameters due to discontinuity of the BeiDou observations, which are discussed in this study. In this section, the theory of LEO POD is briefly introduced.

4.1. Theory of Reduce-Dynamic Orbit Determination

The reduced-dynamic model for the LEO POD has been the mainstream method, which combined the GNSS observations and the dynamic models for LEO POD. To reduce the computation complexity, a few empirical forces or pseudo-stochastic parameters are introduced into the system to assimilate the effect of unmodeled forces. Hence, the pseudo-stochastic parameters are critical for the LEO POD. The precise point positioning (PPP) model is used for involving the GNSS observations, while the LEO observations are not perturbed by the tropospheric delay. The motion equation of the LEO satellite can be expressed as follows:

$$\ddot{\mathbf{r}} = -GM\frac{\mathbf{r}}{r^3} + \mathbf{f}_1(t, \mathbf{r}, \dot{\mathbf{r}}, Q_1, \dots, Q_d, P_1, \dots, P_s) \doteq \mathbf{f} \tag{3}$$

where the GM is the product of the constant of gravity and the mass of Earth, \mathbf{r} is the geocentric radius vector, $\dot{\mathbf{r}}$ is the velocity of the LEO satellite, with the initial condition $\mathbf{r}^{(k)}(t_0) = \mathbf{r}^{(k)}(a, e, i, \Omega, \omega, T_0; t_0)$, $k = 0, 1$, whereas $a, e, i, \Omega, \omega, T_0$ represent the six Keplerian elements at the time t_0 . \mathbf{f}_1 is the perturbing acceleration, and \mathbf{f} is the total acceleration. Q_1, \dots, Q_d represent the force model parameters, and P_1, \dots, P_s represent the pseudo-stochastic orbit parameters. There are different kinds of pseudo-stochastic orbit parameters, such as instantaneous velocity changes, piecewise constant accelerations, and piecewise linear accelerations. Usually, instantaneous velocity pulses and piecewise constant accelerations are adopted in the orbit improved and final orbit determination procedure, respectively. For the instantaneous velocity changes added at epoch t_i in the direction $\mathbf{e}(t)$, the pseudo-stochastic parameter $P_i = V_i$ in Equation (3) is written as $P_i = V_i \cdot \delta(t - t_i) \cdot \mathbf{e}(t)$, and the $\delta(t)$ is Dirac's delta function. Moreover, the piecewise constant accelerations are generally adopted as

the empirical accelerations for orbit determination. Adding the change of acceleration a_i in direction $e(t)$ during the time $t_{i-1} < t < t_i$, the pseudo-stochastic parameter $P_i = a_i$ in Equation (3) is written as $P_i = a_i \cdot e(t)$.

4.2. POD Strategy of Luojia-1A Satellite

The reduced dynamic orbit determination method is used for Luojia-1A satellite POD. In the data processing, both code and carrier-phase observations are used to form the ionosphere-free linear combination, and the observations are resampled into 5 s. The details of the data processing strategies for Luojia-1A satellite POD are presented in Table 1

Table 1. The data processing strategies for Luojia-1A satellite POD.

| Type of Parameter | Settings |
|---|---|
| Observations | BDS B1 and B2 code and carrier-phase observations |
| Sample rate | 5 s |
| Cut off angle | 0° |
| BeiDou antenna phase center | PCV.atx [27] |
| Relativistic effects | IERS 2010 |
| Ionospheric error | Ionosphere-free linear combination |
| Earth rotation | ERP products Provided by Wuhan University |
| Nutation | IAU2000R06 |
| Polar motion | IERS2010XY |
| BeiDou precise orbit and clock products | WUM products Provided by Wuhan University |
| Earth's gravity field | EGM2008 model with the degree of 120 |
| Solid Earth tides | IERS 2010 |
| Ocean tides | FES 2004 |
| Planetary calendar | DE405 |
| Solar pressure | ECOM |
| Pseudo-stochastic parameters | Radial, along-track, and cross-track directions |

5. Luojia-1A Satellite POD Results and Discussion

5.1. The Procedure of Luojia-1A Satellite POD

Several steps are required for the procedure of Luojia-1A satellite reduced dynamic orbit determination, which can be briefly described as follows. Firstly, obtaining the prior orbit of the satellite using the BDS pseudorange observations. The precise orbit and clocks products of BeiDou satellites, as well as the ERP products, are adopted to process the pseudorange positioning orbit result and then fitting the prior orbit using numerical integration. Secondly, data preprocessing for the zero difference phase observations, including cycle slip detection and outlier detection. After that, estimate the orbital parameters, dynamic parameters, and the pseudo-stochastic parameters for solving the improved satellite orbit, which is determined based on the prior orbit and the screened phase observations. The data preprocessing as well as the orbit improving procedure are iterated for the precise solution. Finally, the orbit generated from the last step is introduced as the prior orbit, and the screened phase observations are used to estimate the parameters; thus, the precise orbit result is obtained.

With regards to the orbit precision evaluation method, the overlapping comparison method is used since the Luojia-1A satellite does not equip with the laser reflector array (LRA), and there is no precise reference orbit for comparison. The overlapping comparison strategy for the Luojia-1A satellite is illustrated in Figure 7. The observations of the Luojia-1A satellite in 2018 DOY159 are divided into two observational arcs, one contains the begin epoch until 9:00:30, the other contains 2:14:52 until the last epoch, and then two observational arcs are determined respectively. Therefore, the difference of two solutions in the overlapped part is used to assess the Luojia-1A orbit precision in this study.

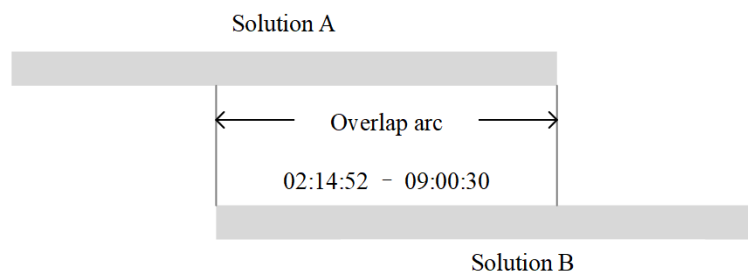


Figure 7. The concept of overlap comparison for the Luojia-1A precise orbit.

5.2. Precise Orbit Determination with BeiDou Observations

The precise orbit determination of LEO requires precise BeiDou orbit, satellite clocks, and earth rotation parameters (ERP) products. One of the challenges for Beidou-based LEO POD is that the BeiDou orbit is generally not as good as the GPS orbit for many reasons. Presently, several analysis centers are providing multi-GNSS precise products with BeiDou constellation support. Four types of BeiDou precise products from different multi-GNSS experiment (MGEX) analysis centers are listed in Table 2. However, a few issues arise in applying these products at the current stage, such as that the Technische Universität München (TUM) products currently does not involve the ERP products. The precise products provided by CODE do not involve the BDS-2 GEO satellites. The German Research Centre for Geosciences (GFZ) and Wuhan University provide the full BDS-2 satellites orbit and clock, but different phase center variation (PCV) models are applied for different ACs, so the products are not directly compatible. In this study, the Wuhan University Multi-GNSS (WUM) products are adopted to determine the precise orbit of the Luojia-1A satellite.

Table 2. The information about BDS orbit and clock products.

| Institution | Indicate | Constellations | Orbit | Clocks | ERP |
|-------------|----------|-----------------------------|--------|------------|------|
| CODE | COM | GPS + GLO + GAL + BDS + QZS | 5 min | 30 s/5 min | 12 h |
| GFZ | GBM | GPS + GLO + GAL + BDS + QZS | 15 min | 30 s/5 min | 24 h |
| WHU | WUM | GPS + GLO + GAL + BDS + QZS | 15 min | 30 s/5 min | 24 h |
| TUM | TUM | GAL + BDS + QZS | 5 min | 5 min | / |

The BDS precise orbit and clocks products are critical factors for the Luojia-1A satellite POD. As reported, the precise orbit products of BDS GEO satellites are not as good as the IGSO and MEO satellites due to poor geometry relationship between the ground stations and the GEO satellites. Generally, the BeiDou GEO precise orbit only achieves a few decimeters accuracy, whereas the IGSO and MEO satellites achieve centimeter-level accuracy. Consequently, adopting the GEO satellites might decrease the LEO POD precision. WUM product employs a three-day arc for BDS orbit determination, and only the middle day is adopted as the final product. So the discontinuity is inevitably present at the day boundary (DBD) in orbit products [27], which can be used to roughly evaluate the orbit precision [28]. To analyze the orbit precise of BeiDou satellites, the average DBDs of 2018 DOY 153 to DOY 163 are calculated. Since the last epoch of WUM orbit products is 23h 45m, the orbit is extrapolated to the 24 h at midnight, then the difference is calculated at the day boundary with the next day orbit product in radial, along-track, and cross-track directions. After that, the average 3D DBDs of BDS satellites orbit products are shown in Figure 8. According to the figure, the GEO satellites present more significant DBDs than the IGSO and MEO satellites. The average DBDs of GEO satellites vary between 58 cm and 130 cm. As for IGSO satellites, the DBDs are less than 50 cm. The DBDs of MEO satellites are the smallest, which is generally less than 20 cm. The statistic result of different types of the BeiDou satellites are listed in Table 3, the average DBD of GEO satellites is 82.28 cm, which is more than three times of IGSO satellites. The precision of MEO satellites is best, which is 17 cm.

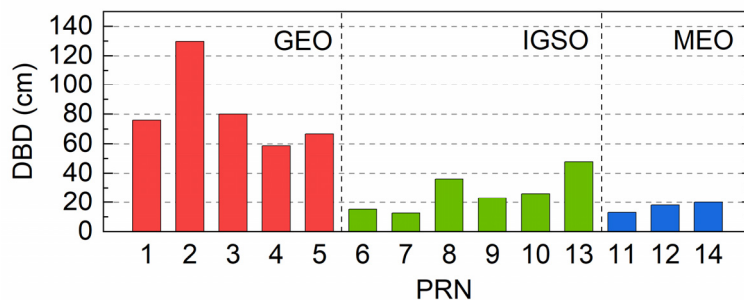


Figure 8. The average day boundary of BDS orbit products.

Table 3. The average 3D day boundary of different orbital type of BeiDou satellites (Unit: cm).

| | GEO | IGSO | MEO |
|--------|-------|-------|-------|
| 3D DBD | 82.28 | 26.74 | 17.00 |

According to the analysis of BeiDou satellites DBDs, the precision of GEO satellites orbit is not as good as that of IGSO and MEO satellites. Therefore, adopting the GEO satellite observations as same as IGSO and MEO satellite observations might decrease the LEO POD precision. Li et al. [22] improve the BDS-based precise orbit determination result of FY-3C by excluding the GEO satellite observations. However, the GEO satellite observations of the Luojia-1A satellite contribute to more than 40% observations. Excluding the GEO satellite observations will dramatically reduce the number of effective observations and lead to a negative effect on the reliability of the POD results.

To determine the precise orbit of the Luojia-1A satellite, the satellite state vector can be expressed as follows [29]:

$$x(t) = (r(t), v(t), p, q)^T \tag{4}$$

where $r(t)$ and $v(t)$ are the position and the velocity of the LEO satellite at epoch t . p represents the force model parameter, e.g., the scaling factors of the perturbing accelerations acting on the LEO satellite. q is the pseudo-stochastic orbit parameter, which compensates for the inaccuracy force model. The observations equation can be briefly described as

$$z = h(x_0) + \varepsilon \tag{5}$$

where z is the n -dimensional observation vector and x_0 is the initial state vector. The recursive least-square estimator is adopted in LEO POD and the weighted least-squares can be written as:

$$\Delta x_0^{lsq} = (H^T W H)^{-1} (H^T W \Delta z) \tag{6}$$

where the H matrix is the partial derivatives of the observations concerning the state vector at the reference epoch t_0 , W is the weighting matrix, and $\Delta z = z - h(x_0^{ref})$. Generally, the weight of different satellites observations is usually set as the same:

$$P = \frac{\sigma_0^2}{\sigma_i^2} \tag{7}$$

where the σ_0 is a priori unit weight factor, which is 0.001m in this study. However, as for the BeiDou system, the precision of GEO satellites orbit is not as good as that of IGSO and MEO satellites. To adopt the GEO satellite observations to improve the reliability of the Luojia-1A precise orbit and reduce the effect from the orbit error of GEO satellites, the strategy of estimation that reduces the weight of GEO satellites observations are proposed in this study. To fully discover the effect of the reduced weight strategy, six different weighting strategies are designed and listed in Table 4. In this study, the IGSO

and MEO satellites are treated as the equal-weighted, and the weight of GEO satellite observations is relative to the IGSO and MEO satellite observations; all the IGSO and MEO satellite observations are set unit weight.

Table 4. The weight setting for GEO satellite observations.

| Scheme ID | A | B | C | D | E | F |
|--------------------|---|------|------|-------|-------|--------|
| Weighting Strategy | 1 | 1/25 | 1/49 | 1/100 | 1/900 | 1/2500 |

The precise orbit determination results of the Luojia-1A satellite with six different weighting strategies are listed in Table 5, and the equal weight of all satellites strategy is used as the reference; the LEO POD precision can be improved by re-weighting the GEO satellite observations. According to the results, the strategy that reduces the weight of GEO satellites can improve the BDS based Luojia-1A satellite POD significantly. As the weight reduces to 1/49, the improvement of precision can reach 44.21%. Moreover, as the weight of GEO satellites is reduced, the precision of Luojia-1A orbit is also improved gradually. Luojia-1A satellite orbit precision can be improved to 2.316 cm in the 3D direction by reducing the GEO satellite weight down to 1/900, in which the RMS of radial direction is better than 1 cm and the improvement is 63.43% refers to the equal-weight strategy. The POD precision will not be continuously improved as the GEO satellite weight reduces to 1/2500. Therefore, 1/900 is considered as the optimal GEO weighting strategy for the Luojia-1A satellite POD.

Table 5. The precision of Luojia-1A precise orbit results with different GEO weighted strategies (Unit: cm).

| Weight | Radial | Along-Track | Cross-Track | 3D | Improvement |
|--------|--------|-------------|-------------|-------|-------------|
| 1 | 2.02 | 3.32 | 5.00 | 6.333 | / |
| 1/25 | 1.50 | 2.29 | 4.37 | 5.157 | 18.57% |
| 1/49 | 1.28 | 2.20 | 2.45 | 3.533 | 44.21% |
| 1/100 | 1.11 | 2.00 | 1.98 | 3.025 | 52.23% |
| 1/900 | 0.94 | 1.75 | 1.19 | 2.316 | 63.43% |
| 1/2500 | 0.94 | 1.73 | 1.23 | 2.322 | 63.43% |

The overlapping orbit comparison result of the Luojia-1A satellite precise orbit is shown in Figure 9, which represents the LEO orbit computed from the different GEO weighting strategies. The panel (a) presents the overlapped orbit residuals for the all satellite equally weighted cases. The figure shows that orbit presents systematical biases for the whole arc and significant fluctuation presence, especially at the end of the arc. As the weight of the GEO satellites is reduced to 1/25, the fluctuation of orbit error series is dramatically mitigated, but the constant bias on the cross-track direction is still present. Further reducing the weight of the GEO satellites can reduce the constant bias in the cross-track direction. A weight of 1/900 for the GEO satellites is considered as the optimal choice for the Luojia-1A satellite since the orbit error is noticeably reduced and without significant fluctuation. The analysis also indicates that the GEO satellite orbit error may introduce fluctuations and constant bias in the LEO orbit determination.

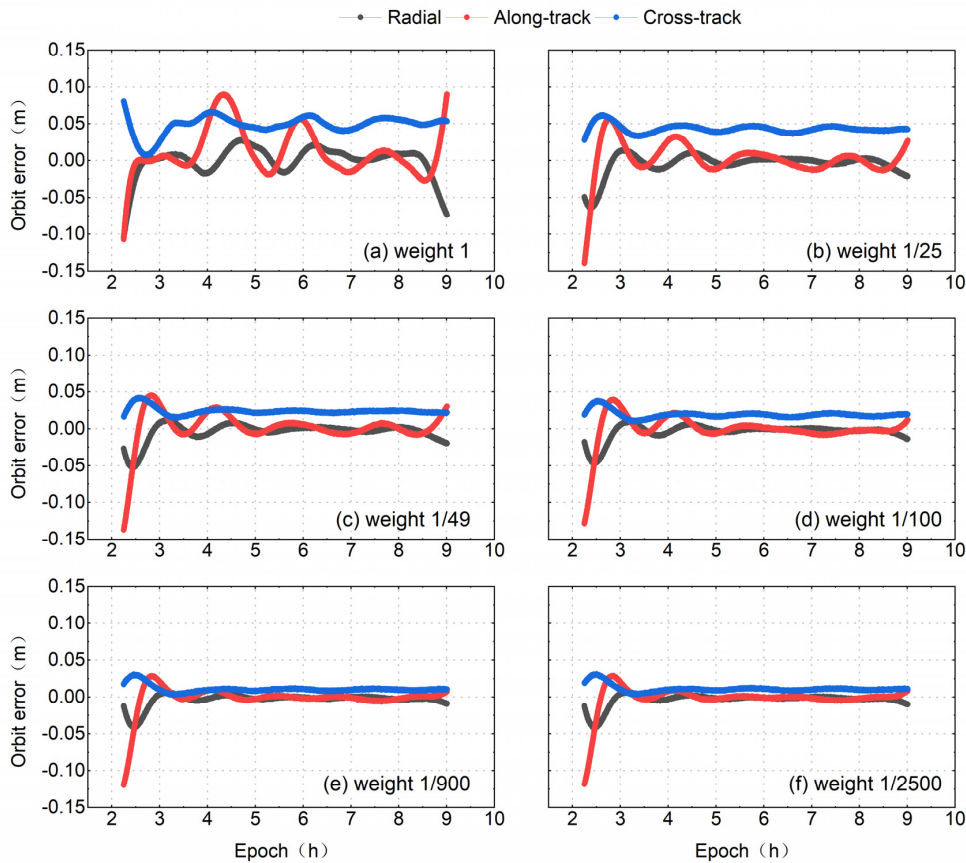


Figure 9. Orbit error of Luojia-1A in different scenarios.

The ionosphere-free carrier phase residuals of Luojia-1A satellite orbit determination under different weight strategy is also analyzed, and the results are presented in Figure 10. In this analysis, the C12 satellite is excluded in the orbit determine procedure due to the absence of precise orbit products. The figure indicates that for the equal weight strategy, the residuals of GEO satellites achieve a minimum while the IGSO and MEO satellites yield larger residuals. By adopting the re-weighting strategy, the residuals of GEO satellites are slightly increased, which is reasonable since the GEO satellite orbit errors are assimilated into the residuals. Meanwhile, the residuals of IGSO and MEO satellites are decreased to less than 10 mm. Different weighting strategies did not lead to dramatic variation of the carrier phase residuals.

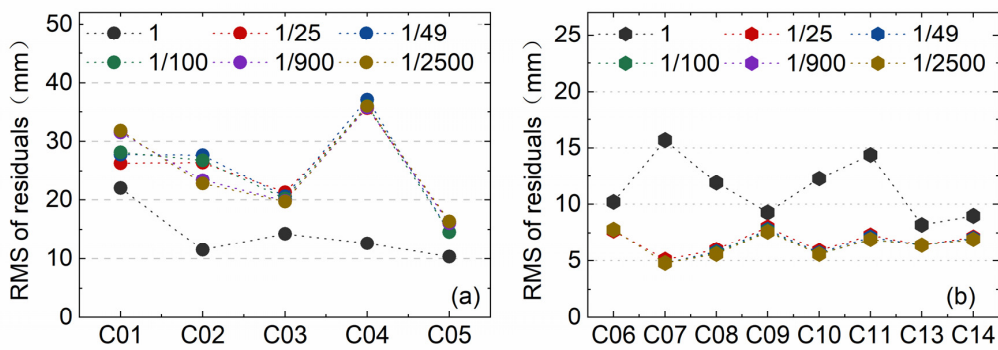


Figure 10. The RMS of different satellite residuals, (a) C01–C05, (b) C06–C14.

The residuals of observations reflect the consistency of the reduce-dynamic model and the observation model, which can approach noise level if only the reduce-dynamic model can represent the

motion of the LEO satellites appropriately. According to experiments, the precise orbit of the Luojia-1A satellite can obtain the best result with the condition that the weight of GEO satellite observations is set 1/900.

The left panel of Figure 11 reflects the relationship between the carrier phase residuals and the elevation angle of the optimal results of the Luojia-1A satellite, which indicates that the residuals are elevation-dependent. For the high elevation angle case, the carrier phase residuals are generally less than 3 cm, while the carrier phase residuals with lower elevation angle are generally smaller than 9 cm. The figure also concludes that the residuals are fairly small in most cases. The carrier phase residuals are smaller than 2 cm in most cases; hence, the overall RMS of residuals is 1.49 cm. According to the right panel, it is apparent that over 70% residuals are smaller than 1 cm and over 93.01% residuals are smaller than 3 cm.

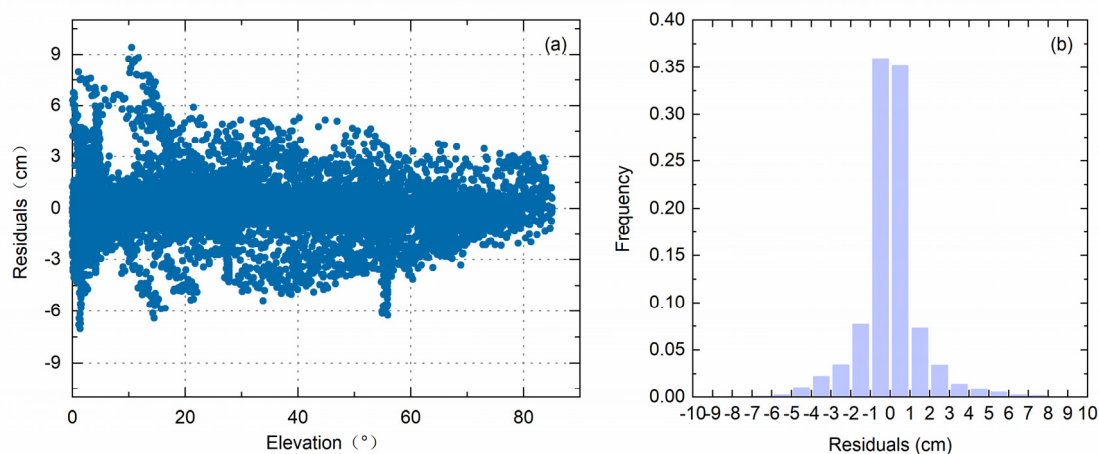


Figure 11. The statistic results of precise orbit determination (POD) residuals. (a) The relationship between POD residuals and the elevation angle. (b) Frequency distribution histogram of POD residuals.

5.3. Tuning the Pseudo-Stochastics Parameters

The Luojia-1A is a nanosatellite which only weighs 19.8 kg. Such a nanosatellite has different dynamic characteristics compared to the large satellites. In the reduced dynamic orbit determination, the pseudo-stochastic parameters are introduced into the orbit determination systems to handle the impact of unmodeled forces. The pseudo-stochastic parameter can assimilate the impact of nuisance forces and prevent the orbit solution divergence.

Usually, different types of pseudo-stochastic parameters are introduced for the precise orbit determination, generally including the instantaneous velocity pulse and the piecewise constant acceleration [30]. The empirical setting of the pseudo-stochastic parameters is adopted in the previous POD experiments, which set up the velocity pulses during the orbit improved procedure and estimate the empirical accelerations in the final POD step. The instantaneous velocity pulses are added every 15 min interval with the prior sigma $5.0 \cdot 10^{-6}$ m/s. The piecewise constant accelerations with the spacing of 6 min are used to improve the orbit result at the last orbit determination procedure, and the prior sigma is 5×10^{-9} m/s². These pseudo-stochastic parameters are added in the radial, along-track, and out-of-plane directions.

In this section, the effect of pseudo-stochastics parameters on the Luojia-1A precise orbit is analyzed by setting different spacing for both the instantaneous velocity pulses and the empirical accelerations. The basic precise orbit determination strategy is listed in Table 1 and the weight of the GEO satellite observations is set 1/900. Five different scenarios of the spacing of pseudo-stochastic parameters are analyzed in this section, including 30 min, 15 min, 10 min, 6 min, and without pseudo-stochastic parameters. The five different spacing strategies are adopted for both the instantaneous velocity pulses and the empirical accelerations. Therefore, there are 25 different mixed strategies in all. The 3D precision of the Luojia-1A precise orbit with different settings for the pseudo-stochastic parameters is shown in

Figure 12. The bottom axis reflects the spacing for the empirical accelerations in the final POD step, whereas the bar in different colors represents different spacing for the instantaneous velocity pulses in the orbit-improved procedure. The figure indicates that the impact of the empirical accelerations is greater than that of the instantaneous velocity pulse. Once the empirical accelerations are absent in the final POD step, the precision of the LuoJia-1A orbit is dramatically decreased. The precision is improved significantly even with the sparse parameters of accelerations. According to the results, the shorter spacing adopted for the piece constant acceleration, the more accurate result is obtained. However, there are no pronounced advantages from the instantaneous velocity pulse for precise orbit determination of the LuoJia-1A satellite. The optimal result of the LuoJia-1A satellite accessed by adopting the strategy with 6 min interval piecewise-constant accelerations parameters and without instantaneous velocity pulse, which achieves the precision of nearly 2 cm in 3D direction. The empirical strategy adopted in the previous experiments can achieve the near-optimal result.

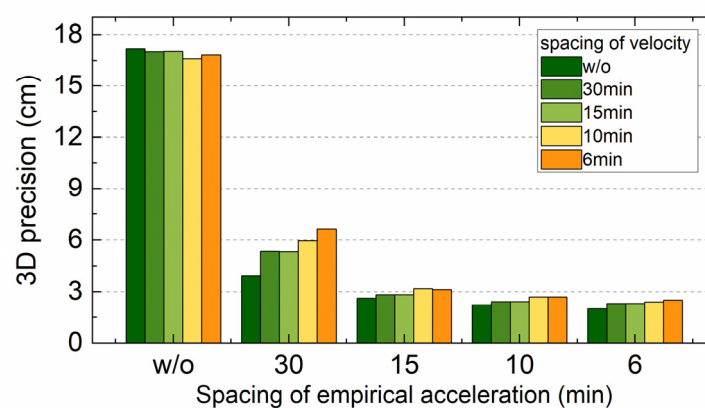


Figure 12. The 3D precision of LuoJia-1A with different settings for the pseudo-stochastic parameters.

As shown in Figure 12, the piece constant acceleration is crucial for the precise orbit determination of the LuoJia-1A satellite. Therefore, the results of the strategies with different spacing of the piecewise constant accelerations but without the instantaneous velocity pulse are further analyzed. The statistic results of LuoJia-1A satellite orbit in the radial, along-track, and cross-track directions are listed in Table 6, and the detail of the orbit error is shown in Figure 13. Panel (a) shows the error of the LuoJia-1A satellite orbit without adding any pseudo-stochastic parameters. The fluctuation of the along-track error is pronounced, in which the error of the start epoch is larger than 30 cm. In the cross-track direction, there is nearly 10 cm constant error. As shown in the other three panels, the errors of three directions are reduced by adding the pseudo-stochastic parameters. The shorter spacing that the piece constant parameters are set, the more precise the result of LuoJia-1A satellite orbit achieved, especially in the beginning of overlap comparison.

Table 6. The RMS precision of LuoJia-1A with different piecewise constant accelerations intervals (Unit: cm).

| Accelerations Interval | Radial | Along-Track | Cross-Track | 3D |
|------------------------|--------|-------------|-------------|--------|
| w/o | 2.43 | 11.17 | 12.83 | 17.184 |
| 30 min | 1.30 | 3.66 | 0.62 | 3.933 |
| 15 min | 0.84 | 2.37 | 0.77 | 2.630 |
| 10 min | 0.74 | 1.99 | 0.73 | 2.245 |
| 6 min | 0.99 | 1.66 | 0.52 | 2.002 |

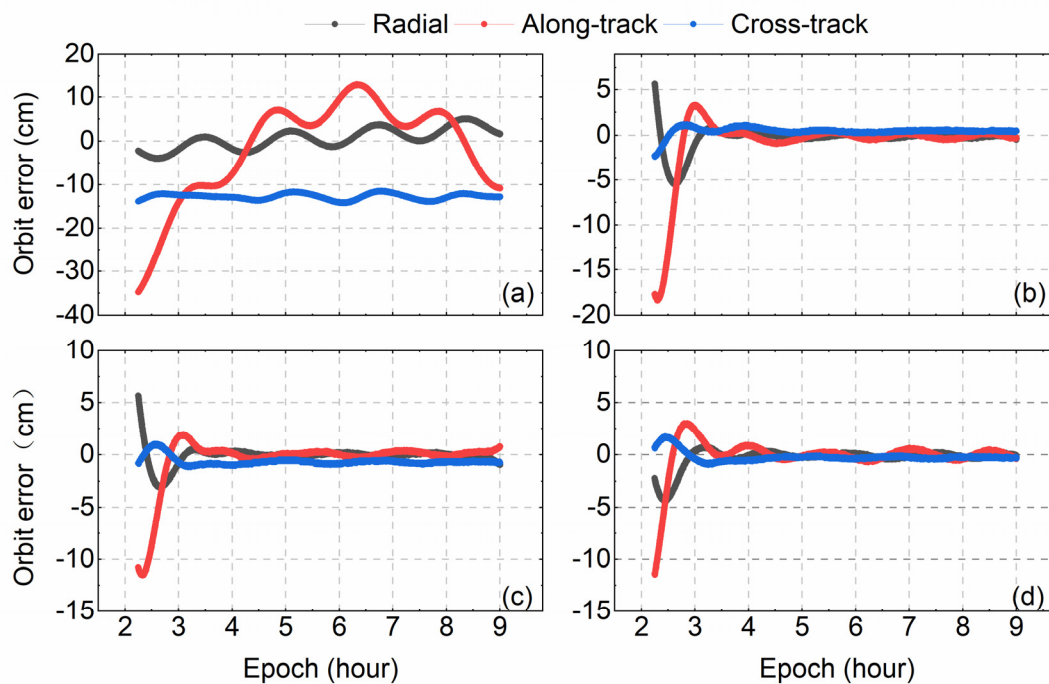


Figure 13. The error of Luojia-1A satellite orbit with different piecewise constant acceleration parameter strategies. (a) Without piecewise constant accelerations. (b) 30 min interval. (c) 15 min interval. (d) 6 min interval.

6. Conclusions

This study focuses on the precise orbit determination of the Luojia-1A low earth orbit satellite with onboard BDS observations. The onboard BDS observations are analyzed firstly and demonstrated that the visibility and continuity of the Luojia-1A are good enough for precise orbit determination. Moreover, the multipath error of onboard BDS code observations is modeled, which shows evident elevation-dependent code bias for the multipath. An elevation-dependent code bias model using LEO data is established, which is capable of modeling the elevation-dependent code bias for the Beidou GEO satellites. The daily boundary of the BeiDou orbit product is calculated and demonstrates that the precision of the GEO satellite orbit is not as good as IGSO and MEO satellites. To overcome the poor precision of the GEO satellite orbit, the strategy that reduces the weight of GEO satellite observations is adopted. The precise orbit result is obtained by adopting the reduced weight strategy, which can achieve 2.3 cm precision by reducing the weight of GEO satellites down to 1/900, whereas the normal equal weight strategy only achieves the 3D precision of 6.3 cm. Finally, the effect of pseudo-stochastic parameters is explored, and the optimal 3-dimensional orbit precision of the Luojia-1A can achieve 2 cm. The strategy that reduces the weight of GEO satellite observations is effective for the precise orbit determination of the Luojia-1A Satellite.

Author Contributions: L.W. created the idea and contributed to writing the manuscript. B.X. wrote the first draft and carried out the experiment. W.F., R.C., and T.L. helped to carry out the data analysis. Y.H. and H.Z. helped to carry out the experiments. All authors have read and agreed to the published version of the manuscript.

Funding: This research was supported by the National Natural Science Foundation of China (No. 41704002, 91638203 and 41904038) and the China Postdoctoral Science Foundation (No. 2017M620337 and 2019M662713). This work is also partially funded by the Fundamental Research Funds for the Central Universities.

Conflicts of Interest: The authors declare no conflict of interest.

References

1. Perosanz, F.; Marty, J.C.; Balmino, G. Dynamic orbit determination and gravity field model improvement from GPS, DORIS and Laser measurements on TOPEX/POSEIDON satellite. *J. Geod.* **1997**, *71*, 160–170. [[CrossRef](#)]
2. Bi, Y.; Yang, Z.; Zhang, P.; Sun, Y.; Bai, W.; Du, Q.; Yang, G.; Chen, J.; Liao, M. An introduction to China FY3 radio occultation mission and its measurement simulation. *Adv. Space Res.* **2012**, *49*, 1191–1197. [[CrossRef](#)]
3. Hackel, S.; Montenbruck, O.; Steigenberger, P.; Balss, U.; Gisinger, C.; Eineder, M. Model improvements and validation of TerraSAR-X precise orbit determination. *J. Geod.* **2017**, *91*, 1–16. [[CrossRef](#)]
4. Li, B.; Ge, H.; Ge, M.; Nie, L.; Shen, Y.; Schuh, H. LEO enhanced Global Navigation Satellite System (LeGNSS) for real-time precise positioning services. *Adv. Space Res.* **2018**, *63*, 73–93. [[CrossRef](#)]
5. Wang, L.; Chen, R.; Li, D.; Zhang, G.; Shen, X.; Yu, B.; Wu, C.; Xie, S.; Zhang, P.; Li, M.; et al. Initial Assessment of the LEO Based Navigation signal augmentation System from Luojia-1A Satellite. *Sensors* **2018**, *18*, 3919. [[CrossRef](#)] [[PubMed](#)]
6. Li, X.; Ma, F.; Li, X.; Lv, H.; Bian, L.; Jiang, Z.; Zhang, X. LEO constellation-augmented multi-GNSS for rapid PPP convergence. *J. Geod.* **2019**, *93*, 749–764. [[CrossRef](#)]
7. Wang, L.; Li, D.; Chen, R.; Fu, W.; Shen, X.; Jiang, H. The Low Earth Orbiter (LEO) Navigation Augmentation Technique-Opportunities and Challenges. *Strateg. Study CAE* **2020**, *22*, 1–12.
8. Ge, H.; Li, B.; Ge, M.; Zang, N.; Nie, L.; Shen, Y.; Schuh, H. Initial Assessment of Precise Point Positioning with LEO Enhanced Global Navigation Satellite Systems (LeGNSS). *Remote Sens.* **2018**, *10*, 984. [[CrossRef](#)]
9. Li, X.; Lv, H.; Ma, F.; Li, X.; Liu, J.; Jiang, Z. GNSS RTK Positioning Augmented with Large LEO Constellation. *Remote Sens.* **2019**, *11*, 228. [[CrossRef](#)]
10. Wang, L.; Li, D.; Chen, R.; Fu, W.; Shen, X.; Jiang, H.; Hao, J. Low Earth Orbiter (LEO) Navigation Augmentation: Opportunities and Challenges. *Chin. J. Eng. Sci.* **2020**, *22*, 144.
11. Yang, Y. Concepts of Comprehensive PNT and Related Key Technologies. *Acta Geod. Cartogr. Sin.* **2016**, *45*, 505–510.
12. Li, D.; Shen, X.; Li, D.; Li, S. On Civil-Military Integrated Space-Based Real-Time Information Service System. *Geomat. Inf. Sci. Wuhan Univ.* **2017**, *42*, 1501–1505.
13. Wang, L.; Chen, R.; Xu, B.; Zhang, X.; Li, T.; Wu, C. The Challenges of LEO Based Navigation Augmentation System Lessons Learned from Luojia-1A Satellite. In *China Satellite Navigation Conference (CSNC) 2019 Proceedings*; Springer: Beijing, China, 2019; pp. 298–310.
14. Bertiger, W.; Bar-Sever, Y.; Christensen, E.; Davis, E.; Guinn, J.; Haines, B.; Ibanez-Meier, R.; Jee, J.; Lichten, S.; Melbourne, W.; et al. GPS precise tracking of TOPEX/Poseidon: Results and implications. *J. Geophys. Res.* **1994**, *99*, 24449–24464. [[CrossRef](#)]
15. Van den Ijssel, J.; Visser, P.; Patiño Rodriguez, E. Champ precise orbit determination using GPS data. *Adv. Space Res.* **2003**, *31*, 1889–1895. [[CrossRef](#)]
16. Jäggi, A.; Hugentobler, U.; Bock, H.; Beutler, G. Precise orbit determination for GRACE using undifferenced or doubly differenced GPS data. *Adv. Space Res.* **2007**, *39*, 1612–1619. [[CrossRef](#)]
17. Bock, H.; Jäggi, A.; Švehla, D.; Beutler, G.; Hugentobler, U.; Visser, P. Precise orbit determination for the GOCE satellite using GPS. *Adv. Space Res.* **2007**, *39*, 1638–1647. [[CrossRef](#)]
18. Montenbruck, O.; Hackel, S.; van den Ijssel, J.; Arnold, D. Reduced dynamic and kinematic precise orbit determination for the Swarm mission from 4 years of GPS tracking. *Gps Solut.* **2018**, *22*, 79. [[CrossRef](#)]
19. Montenbruck, O.; Hauschild, A.; Steigenberger, P.; Hugentobler, U.; Teunissen, P.; Nakamura, S. Initial assessment of the COMPASS/BeiDou-2 regional navigation satellite system. *GPS Solut.* **2013**, *17*, 211–222. [[CrossRef](#)]
20. Zhang, X.; Wu, M.; Liu, W.; Li, X.; Yu, S.; Lu, C.; Wickert, J. Initial assessment of the COMPASS/BeiDou-3: New-generation navigation signals. *J. Geod.* **2017**, *91*, 1225–1240. [[CrossRef](#)]
21. Chen, X.; Zhao, S.; Wang, M.; Lu, M. Space-borne BDS receiver for LING QIAO satellite: Design, implementation and preliminary in-orbit experiment results. *GPS Solut.* **2016**, *20*, 837–847. [[CrossRef](#)]
22. Li, M.; Li, W.; Shi, C.; Jiang, K.; Guo, X.; Dai, X.; Meng, X.; Yang, Z.; Yang, G.; Liao, M. Precise orbit determination of the Fengyun-3C satellite using onboard GPS and BDS observations. *J. Geod.* **2017**, *91*, 1313–1327. [[CrossRef](#)]

23. Zhang, Q.; Guo, X.; Qu, L.; Zhao, Q. Precise Orbit Determination of FY-3C with Calibration of Orbit Biases in BeiDou GEO Satellites. *Remote Sens.* **2018**, *10*, 382. [[CrossRef](#)]
24. Wanninger, L.; Beer, S. BeiDou satellite-induced code pseudorange variations: Diagnosis and therapy. *GPS Solut.* **2015**, *19*, 639–648. [[CrossRef](#)]
25. Wang, L. Reliability Control of GNSS Carrier-Phase Integer Ambiguity Resolution. Ph.D. Thesis, Queensland University of Technology, Brisbane, Australia, 2015.
26. Wang, L.; Feng, Y.; Wang, C. Real-Time Assessment of GNSS Observation Noise with Single Receivers. *J. Glob. Position Syst.* **2013**, *12*, 73–82.
27. Guo, J.; Xu, X.; Zhao, Q.; Liu, J. Precise orbit determination for quad-constellation satellites at Wuhan University: Strategy, result validation, and comparison. *J. Geod.* **2016**, *90*, 143–159. [[CrossRef](#)]
28. Griffiths, J.; Ray, J.R. On the precision and accuracy of IGS orbits. *J. Geod.* **2009**, *83*, 277–287. [[CrossRef](#)]
29. Montenbruck, O.; Gill, E. Lutz F. Satellite orbits: Models, methods, and applications. *Appl. Mech. Rev.* **2002**, *55*, B27–B28. [[CrossRef](#)]
30. Jäggi, A.; Hugentobler, U.; Beutler, G. Pseudo-Stochastic Orbit Modeling Techniques for Low-Earth Orbiters. *J. Geod.* **2006**, *80*, 47–60. [[CrossRef](#)]



© 2020 by the authors. Licensee MDPI, Basel, Switzerland. This article is an open access article distributed under the terms and conditions of the Creative Commons Attribution (CC BY) license (<http://creativecommons.org/licenses/by/4.0/>).